Interactive Training System for Interventional Electrocardiology Procedures

Hugo Talbot, Federico Spadoni, Christian Duriez, Maxime Sermesant, Stéphane Cotin, Hervé Delingette

Interactive Training System for Interventional Electrocardiology Procedures

Hugo Talbot[a], Federico Spadoni[a], Christian Duriez[a], Maxime Sermesant[a], Mark O'Neill[b], Pierre Jaïs[c], Stéphane Cotin[a], Hervé Delingette[a]

[a] *Inria, France*
[b] *Department of Cardiology, Guy's and St. Thomas' NHS, London, United Kingdom*
[c] *Hôpital Haut-l'évêque - IHU Liryc, Bordeaux, France*

Abstract

Recent progress in cardiac catheterization and devices has allowed the development of new therapies for severe cardiac diseases like arrhythmias and heart failure. The skills required for such interventions are very challenging to learn, and are typically acquired over several years. Virtual reality simulators may reduce this burden by allowing trainees to practice such procedures without risk to patients. In this paper, we propose the first training system dedicated to cardiac electrophysiology, including pacing and ablation procedures. Our framework involves the simulation of a catheter navigation that reproduces issues intrinsic to intra-cardiac catheterization, and a graphics processing unit (GPU)-based electrophysiological model. A multi-threading approach is proposed to compute both physical simulations (navigation and electrophysiology) asynchronously. With this method, we reach computational performances that account for user interactions in real-time. Based on a scenario of cardiac arrhythmia, we demonstrate the ability of the user-guided simulator to navigate inside vessels and cardiac cavities with a catheter and to reproduce an ablation procedure involving: extra-cellular potential measurements, endocardial surface reconstruction, electrophysiology mapping, radio-frequency (RF) ablation, as well as electrical stimulation. A clinical evaluation assessing the different aspects of the simulation is presented. This works is a step towards computerized medical learning curriculum.

Keywords: Real-Time Electrophysiology, Endovascular Navigation, Training Simulator, Interactive Simulation.

1. Introduction

Cardiac arrhythmia and heart failure are life-threatening pathologies. Cardiac arrhythmia is an abnormal electrical activity in the myocardium (heart muscle), whereas heart failure occurs when the heart can not pump sufficiently to meet the need of the body. Since cardiac electrophysiology induces the contraction of the cardiac muscle, any abnormal electrical stimulation pattern may lead to abnormal contractions of the heart potentially causing heart failure. Depending on the pathology, different therapies are pursued. RF ablation is performed for ventricular tachycardia, whereas Cardiac Resynchronization Therapy (CRT) is preferred in case of severe heart failure. In this paper, we only consider ventricular extrasystole, i.e. ventricular tachycardia caused by ectopic foci. An ectopic focus is an abnormal pacemaker area (outside of the sinoatrial node) that initiates abnormal self-generated beats. Such pathologies can occur due to changes in the heart structure subsequent to a coronary artery disease or as chronic consequences of hypertension, diabetes or cardiomyopathy, as stated in Maron et al. (2006).

The use of minimally invasive techniques is now widespread in many medical fields. Cardiology is no exception. However, less invasive interventions often implies more complex pathways to reach the region of interest. Considering ectopic foci located inside the right ventricle (RV), the procedure first consists of inserting catheters in the femoral vein which allows direct access to the right atrium (RA). Under fluoroscopic imaging, endovascular navigation not only requires an in-depth knowledge of the vascular system but also good hand-eye coordination. Once the RA is reached, the catheter

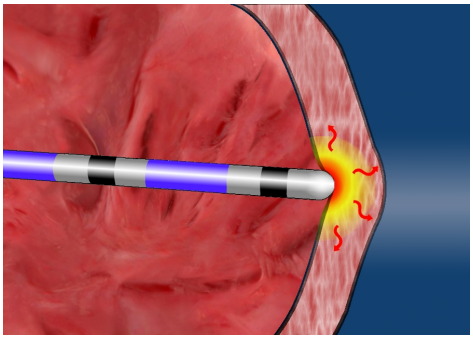

Figure 1: RF ablation: the catheter heats the endocardial surface to damage the tissues responsible for the pathology

(a) A cath lab (from www.medwow.com)

(b) Our setup using the Mentice VIST device

Figure 2: Comparison of our setup with a catheterization laboratory: aiming at an immersive experience, our training system is based on a "cath lab"-like environment

must be skillfully handled in order to access the RV through the tricuspid valve. The electrophysiologist must then perform a 3D reconstruction of the RV endocardial surface. Afterwards, the recording of the electrical activity is performed by acquiring a map of activation times. The ectopic focus includes an excitable group of cells initiating a premature (ectopic) heart beat with a specific electrical pattern. Ectopic beats often appear sporadically and several steps are required to define the exact location of the pathological cells. Latest electrophysiology mapping systems are able to automatically detect an ectopic pattern from the analysis of the body surface ECG. As soon as an ectopic beat occurs, the system computes and maps the local activation time on the 3D reconstructed endocardial surface. By scanning the entire cavity, the pathological area can be localized and ablated since the ectopic focus corresponds to the region with the earliest activation time. As illustrated in Figure 1, RF ablation consists in heating the ectopic focus that leads to its cellular death, thus suppressing the related abnormal beats. RF ablation is frequently preferred to other ablation techniques (high intensity focused ultrasounds, cryotherapy) for cardiac arrhythmia, but the success rate of the procedure remains unsatisfactory: between 50 and 90 % of success, whereas the rate of late recurrence amounts to 20 up to 40 %. According to Aliot et al. (2009), the long-term success rates of RF ablation in the context of scar-related VT even falls between 30 and 60 %. In their paper, authors point out a lack of clinical consensus on the optimum RF ablation strategy, which could explain these unstable success rates.

Until now, residents in cardiology train on patients by separately learning each step of the procedure under the supervision of a senior cardiologist. In order to shorten the training period and to allow a virtual training on complex patient cases, we propose a training system for interventional cardiology based on the simulation of electrophysiology.

Specifications. First, an endovascular catheterization must be provided in the training so that cardiology interns practice navigation in minimally invasive conditions. Then, the biophysical simulation has to reproduce the cardiac electrophysiology as realistically as possible. The trainee can then interact with the simulated electrophysiology, i.e. analyzing the extra-cellular potentials, mapping activation times on the reconstructed endocardium and ablating the arrhythmia. Using our simulation framework for virtual training aims to achieve accurate and fast computations of both navigation and electrophysiology. In this computation, spatial and temporal discretizations must be sufficiently small to reliably reproduce the effect of an ectopic focus, whereas computational efficiency is key to ensure interactivity while navigating inside the blood vessels or interacting with the cardiac electrophysiology (e.g. intra-cardiac measurements, RF ablation or electrical stimulation). To make this framework even more immersive, the simulation environment has to mimic the environment of the operating room.

Previous work. Previous research projects have led to training simulators in cardiology, as Dawson et al. (2000). The most recent simulator is proposed by Chiang et al. (2013) and focuses on intra-ventricular navigation. The contribution of this work consists in virtually reproducing the conditions for the slip and nonslip interaction of the catheter. Authors present a qualitative analysis of the catheterization training using experimental data on a porcine left ventricle, as well as a user evaluation. Few training systems succeeded to be commercialized such as Cathi from Siemens (2006), VIST from Mentice (2012), Simantha from SimSuite Corporation (2013), CathLabVR from CAE HealthCare (2013) and Angio Mentor from Simbionix (2012). These simulators mostly focus on endovascular navigation and include pre-recorded electrocardiograms (ECG), but none of these simulators includes a biophysical modeling of the cardiac electrophysiology, or models the interaction between a catheter and cardiac electrophysiology.

Simulating the human cardiac electrophysiology is a wide field of research. However, only recent work by Talbot et al. (2013a); Rapaka et al. (2012); Bartocci et al. (2011) investigate high performance computing applied to cardiac

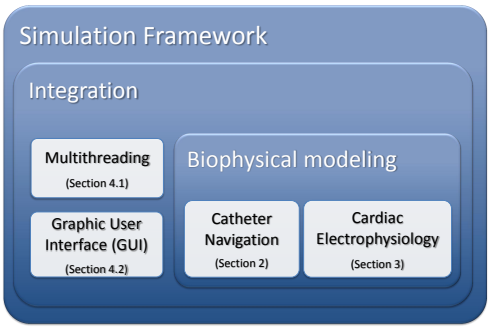

Figure 3: Overview of the structure of the paper

electrophysiology in order to achieve quasi real-time simulations. Therefore, coupling both a simulation of endovascular navigation and a model of cardiac electrophysiology while keeping performances close to real-time is extremely challenging.

Proposed framework. We present a training system dedicated to interventional electrocardiology procedures that combines endovascular catheterization with a biophysical modeling of cardiac electrophysiology. The proposed endovascular navigation takes place inside a beating heart model using a steerable catheter model. A phenomenological model of cardiac electrophysiology based on a GPU implementation allows reaching a high level of interactivity. Using a multithreading approach, we couple cardiac electrophysiology and catheter navigation simulations, both running separately in real-time but at different time steps. This contribution enables the simulation to meet the requirements related to training systems in terms of computational efficiency and accuracy. With this framework, the user can interactively visualize bipolar potentials, reconstruct the endocardial surface while mapping activation times, and perform RF ablation or electrical stimulation in real-time. Inspired by the setup of a catheterization laboratory (or cath lab, see Figure 2(a)), our framework reproduces fluoroscopic images, and intra-cardiac ECG plots. As shown in Figure 2(b), it also interfaces with a tracking device from Mentice (2012).

This paper is written according to the structure of the training simulator displayed in Figure 3. First, we focus on the catheter navigation in the scope of electrocardiology, i.e. with a moving environment. Second, the computational model chosen to simulate cardiac electrophysiology is presented.

Third, we describe how the navigation and electrophysiology simulation are integrated and interfaced in our framework. Finally, a performance analysis and a clinical evaluation are conducted based on a synthetic case of ventricular extrasystole.

2. Catheter Navigation in Cardiology

The simulator is developed using SOFA[1] Faure et al. (2012) and reproduces an intervention aimed at ablating an ectopic focus located in the RV. In this section, we first provide the background on the catheter navigation model. Then, we present a beating heart model extracted from cine magnetic resonance imaging (MRI) data and its coupling with the collision response process. The section ends with the presentation of our steerable catheter model.

2.1. Background on Catheter Navigation Models

The real-time simulation of the catheter behavior during endovascular procedures is particularly challenging and has been the focus of several research works. Catheters are wire-like structures characterized by stiff and light materials, high tensile strength and low resistance to bending. In continuum mechanics, the behavior of such structures falls into the category of rods. The beam theory, built on Kirchhoff rods hypothesis, is widely used for finite element method (FEM) of such structures and is described in several publications, such as Przemieniecki (1985). This approach is completed by Cosserat et al. (1909) who describe wire-like structures as a set of oriented micro-solids. Starting from these theoretical work, many variations and dedicated algorithms (referenced by Theetten et al. (2008)) have been developed to simulate rod deformation.

Our work relies on the FEM introduced in Duriez et al. (2006) and further developed in Dequidt et al. (2008), both in the context of coil embolization in neurology. This method is based on Kirchhoff rod theory, so that our catheter results in a serial set of beam elements, as it appears in Figure 4. We choose this corotational approach (using 40 beams) because it handles geometric non-linearity due to large changes in the shape of the object. Defined in a Cartesian coordinate system, the contact resolution also results

[1]SOFA is an open source framework for interactive numerical simulations in medicine. More information about SOFA can be found at `http://www.sofa-framework.org`

in the assembly of a block-tridiagonal matrix, which is efficient to solve. Other models exist for wire-like structures as the inextensible super-helices model proposed by Bertails et al. (2006) or a linear representation of angular springs in Wang et al. (2007). However, Bertails' super-helices involve a quadratic time complexity regarding the number of helical elements. In comparison, the corotational beam approach offers a linear complexity. Based on non-physical angular springs, the representation chosen by Wang implies non-physical behavior.

The corotational model assumes that the deformations remain relatively small in a local coordinate frame defined at the level of each element. In our scope of endovascular navigation, the catheter undergoes large displacements but only small deformations, which meets the corotational hypothesis. One beam element is delimited by two nodes having 6 degrees of freedom (DOF) each: 3 angular $\mathbf{q}_r$ and 3 spatial positions $\mathbf{q}_t$. The beam element includes a 12x12 symmetric stiffness matrix $\mathbf{K}_e$ that relates the nodal degrees of freedom of a beam element to the forces and torques applied to them. In the absence of manufacturer specifications, the catheter stiffness is estimated under the supervision of clinical experts of CHU Bordeaux. Starting from a reference stiffness based on the constitutive materials of an ablation catheter, the stiffness is adapted so that the catheter motion in the simulated fluoroscopic and 3D views corresponds to the intra-operative behavior. The homogeneous stiffness of our virtual catheter is finally estimated as $E_{cath} = 2.5\ e^7$ Pa. The final internal forces $\mathbf{f^i}$ generated by the deformation of the structure at one node i are:

$$\mathbf{f}^i = \sum_{e=i-1}^{i} \mathbf{R}_e(\mathbf{q})\ \mathbf{K}_e\ (\mathbf{R}_e(\mathbf{q})^T(\mathbf{q} - \mathbf{q}_e) - \mathbf{p}_{\text{rest}}) \tag{1}$$

where e is the index of the two beams connected to this i^{th} node. In Figure 4, $\mathbf{q_1}$, $\mathbf{q_2}$ and $\mathbf{q_3}$ are the vectors of the 6 DOF position of the three nodes (respectively 1, 2, 3) belonging to the two beams e_1 and e_2 in the global coordinate frame (quaternions are used for rotations). In this figure, tricolor

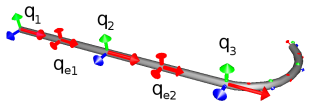

Figure 4: Catheter beam model in its curved rest shape: with the tricolor nodal coordinate frames; and the red frames matching the middle of each beam

frames depict these nodal frames. $\mathbf{q}_{ej}$ denotes the middle frame of the j^{th} beam (red frame) which is computed as an intermediate 6 DOF position between the two nodes of the beam. $\mathbf{p}_{\text{rest}}$ corresponds to the 6 DOF rest position of these nodes in the local coordinate frame. Rotation matrix $\mathbf{R}_e$ is used for the mapping of vectors defined in the local coordinate frame to the global coordinate frame. As the rotation is not the same for the two beams, matrices $\mathbf{R}_e$ cannot be factorized. As a result, the formulation of the internal force is a non-linear function of the nodal positions. We also integrate a mass matrix to obtain a dynamic model and we use a backward Euler integration with a time step of $dt_N = 0.02$ s. This model has been validated experimentally by Dequidt et al. (2008) by studying the coil rest shape under deformation.

The collision response is uni-directional as only the catheter is deformed when it collides against the walls of both vessels and the heart which are considered rigid. The catheter navigation presented in this work focuses on the inferior vena cava. The vena cava belongs to venous system. Veins are significantly less elastic than arteries. Moreover, the inferior vena cava is a large vessel (between 1.5 and 2.5 cm in diameter) and does not deform significantly. The assumption of rigid vessels therefore appears reasonable but can not be extended to navigation in small vessels.

For catheter navigation, the main challenge remains the collision response with the vessel or heart walls. Even with static vessels, quick changes of the catheter velocity and stick/slip transitions generate non-smooth dynamics of the catheter. The collision detection is performed using first a Bounding Volume Hierarchy (BVH) for the broad phase, and then computing local minimal distances, as introduced in Johnson and Willemsen (2004). The simulation model is based on Signorini's and Coulomb's laws that are solved using the constraint-based process described in Duriez et al. (2005) and optimized for catheter navigation in Duriez et al. (2006). For every contact between the catheter and the vessel, we can build a mapping function $\mathbb{A}$ that links the relative positions in the contact space[2] to the motion space. For each contact, $\mathbb{A}$ includes three DOF: one normal component for the contact

[2]The first dimension of the contact space is along the surface normal due to the frictionless response of the Signorini's law. The two other dimensions of the contact space are tangential to the surface according to the Coulomb's friction law.

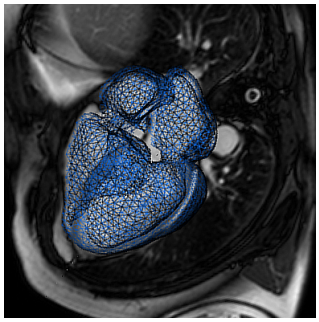

Figure 5: 3D SSFP slice with the static mesh resulting from segmentation (animation is then computed from the 4D cine MRI images)

response and two tangential components characterizing the friction.

$$\boldsymbol{\delta}_\alpha = \mathbb{A}_\alpha(\mathbf{q}, t) - \mathbb{A}_\alpha(\mathbf{x}, t) \tag{2}$$

with $\boldsymbol{\delta}_\alpha$ the relative displacement between the catheter and the vessel walls. $\mathbb{A}_\alpha(\mathbf{q}, t)$ and $\mathbb{A}_\alpha(\mathbf{x}, t)$ are respectively the mapping function of the catheter and the vessel walls. Both depend on the contact α, the catheter position $\mathbf{q}$ and the wall position $\mathbf{x}$.

To obtain a kinematic relation between both contact and motion spaces, we use a linearization of Eq. 2 according to the position of the catheter nodes. Hence, for each contact, we build the Jacobian of the mapping function: $\mathbf{H}_\alpha = \frac{\partial \mathbb{A}_\alpha}{\partial \mathbf{q}}$

In the model, we consider that the motion of the vessel is not influenced by the collision response, so there is no need to compute the Jacobian with respect to the vessel node position. We end up with the formulation of the relative displacements in the contact space:

$$\boldsymbol{\delta} = \underbrace{\mathbb{A}_\alpha(\mathbf{q}^{\text{free}}) - \mathbb{A}_\alpha(\mathbf{x})}_{\boldsymbol{\delta}^{\text{free}}} + \mathbf{H} d\mathbf{q}^{\text{cor}} \tag{3}$$

with $\mathbf{q}^{\text{free}}$ being the *free* position of the catheter (i.e. position obtained when no contact force applies) and $d\mathbf{q}^{\text{cor}}$ being the unknown corrective motions due to collision response. This corrective motion is obtained by solving Eq. 3 based on the Signorini's law through a Linear Complementarity Problem (LCP), as presented by Duriez et al. (2006). A combination with Coulomb's law leads to a Non-linear complementarity problem (NLCP) solved using a Gauss-Seidel algorithm (see Duriez et al. (2005) for details).

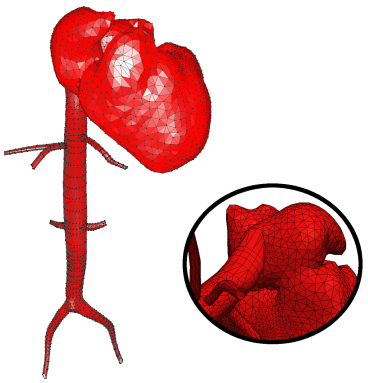

Figure 6: Resulting triangular mesh used for collision detection during cardiovascular navigation, and zoom on the connection between the inferior vena cava and the right atrium

2.2. 4D-Image Based Model of the Heart

In this section, we describe the generation of realistic cardiac motion through time series of images, also called 4D (3D + time) images of the heart. We then describe how this animated mesh is included within the collision pipeline in order to provide a reliable behavior of the catheter.

2.2.1. Beating Heart Model

For a realistic navigation, we first need to recover the cardiovascular structure. Patient data were acquired in the framework of the European euHeart project[3] Talbot et al. (2013b). As shown in Figure 5, 3D MRI are preoperatively obtained in order to reconstruct the patient-specific heart anatomy. Both atria and ventricles are labeled using a plugin tool implemented in GIMIAS[4]. The mask resulting from the segmented steady-state free precession (SSFP) images is then meshed using the CGAL library[5]. With respect to endovascular navigation, a first mesh generation provides us the four heart chambers including 12,950 triangular elements. A second, static and finer mesh, only modeling the ventricles, is extracted for the electrophysiology computation including 30,807 linear tetrahedra.

[3]For more information about the euHeart project: `www.euheart.eu`

[4]GIMIAS is an open source framework providing image visualization, manipulation, and annotation. For more information: `www.gimias.net`

[5]CGAL is an open source software library that provides algorithms in computational geometry. For more information: `www.cgal.org`

However, the catheter navigation step also requires a mesh of the venous system leading to the heart, since navigation starts from the femoral vein. Regarding blood vessels, synthetic data of the inferior vena cava are extracted from the Zygote data set[6]. The resulting mesh for navigation fuses the generic model of vena cava with the patient-specific mesh of the heart (presented in Figure 6).

After re-ordering the cardiac phases (from passive filling to ventricular isovolumetric relaxation), we estimate the cardiac motion from 4D cine MRI information using a Demon-based registration algorithm detailed by Mansi et al. (2011) which includes a penalization of the compressibility of the estimated motion field. This recovered motion is overall reasonable, although it underestimates the tangential motion at the apex due to the aperture problem. The estimated deformation field is resampled onto vertices of the navigation mesh, thus resulting in a realistic beating heart model, ready to be integrated in the simulation of catheter navigation. More important is that the resulting animated mesh stays coherent from one frame to the next, i.e. the mesh topology is retained during the animation. The benefit of this coherent animated mesh will be detailed in the next sections.

2.2.2. Using Heart Motion in the Collision Pipeline

Accounting for the cardiac motion during catheter navigation is key to improve the realism of the simulation. Duriez et al. (2006) and Dequidt et al. (2008) only consider static walls for their endovascular navigation since they concentrate on a neurological application. In the scope of cardiology, navigation becomes more complex due to the motion of the heart. Not only is the heart contracting, but the surrounding vascular system is moving as well. In their simulator, Chiang et al. (2013) achieve a 3D reconstruction of the left ventricular endocardium. The authors focus only on a dynamic left ventricle and the catheter inside it. All other cardiac chambers and the entire length of the catheter (from the femoral vein to the left atrium) are ignored, thus limiting the realism of the simulation. In this paper, we propose an extension of the collision detection from Duriez et al. (2006) handling rigid moving cavities. The catheterization procedure starts from an insertion point in the femoral vein, up to the heart chamber of interest (here, the RV).

[6]The Zygote data are a set of 3D anatomical models sold by the company Zygote Media Group. For more information: `www.zygote.com`

The evaluation of the relative distance between the walls and the catheter is given in Eq. 3. With a static environment, positions of the vessels $\mathbf{x}$ (corresponding to the mesh in Figure 6) remain constant. To account for the cardiac motion, $\mathbf{x}$ therefore needs to be updated at every time step of the navigation. Subsequently, all bounding volume boxes used for collision detection are recomputed. Finally, the relative distance $\boldsymbol{\delta}$ can be re-estimated to compute the collision response, thus accounting for the vessel/heart motion.

In the previous section, the extraction of a coherent and animated mesh from medical images was detailed. Regarding the collision detection, BVH and proximity computations are preferred to distance maps since distance maps would need to be recomputed at each navigation step and previous positions of the catheter are translated into the new map. In our BVH-proximity approach, the conservation of the mesh topology ensures efficiency and more continuity (i.e. stability) since contact properties can be easily maintained from one frame to another. Using an Intel Core i7 central processing unit (CPU), the computation time required for one collision detection step ranges from 3.99 ms to 6.54 ms. High level of performances can therefore be reached but the number of Frames Per Second (FPS) strongly depends on the number of contacts. Below 50 contacts real-time performance is ensured, whereas navigation is twice slower than real-time with more than 100 contacts. Details about the hardware configuration will be given in Section 5.

2.3. Navigation of the Steerable Catheter

To mimic the endovascular navigation, our framework is coupled with the VIST device from Mentice (2012) (see Figure 2(b)), which measures the catheter insertion depth and rotation. This information is conveyed to the simulation and taken into account in real-time to drive the catheter. Providing buttons, pedals as well as joysticks, this device allows us to manage all possible interactions, e.g. moving the C-Arm used for the fluoroscopy.

Catheter navigation is a complex task even when guided with fluoroscopic images. Reaching the heart cavities becomes even more challenging since the heart beats and the path to follow is not straightforward. To go from the RA to the RV, the catheter must bend to face the tricuspid valve. During the intervention as in our simulation, the cardiologist uses a specific steerable catheter, such as the one presented in Figure 7(a). The steerable catheter can use either pneumatic or mechanical actuators. Due to its bending feature, this catheter makes the access to the RV easier.

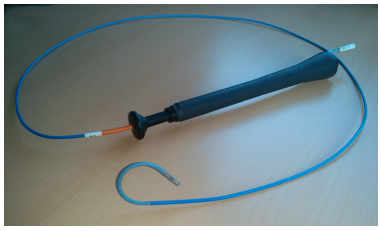

(a) Pneumatic steerable catheter used by cardiologists

(b) Bending motion of the virtual catheter

Figure 7: Comparision of (a) a real catheter used by cardiologists during electrophysiological procedures and (b) our virtual steerable catheter

In order to offer the user the same tools as in the operating room, our catheter model needs to be steerable as well. The catheter geometry is characterized by its rest shape, corresponding to the geometry without any force or constraint applied to the catheter. In our representation, the curvature of the rest shape is parameterized by an angle. The higher the angle, the more the catheter bents. Set to zero, the catheter is straight. Dynamically controlled by the user through the Mentice device (see Figure 7(b)), the curvature can be changed to better navigate inside heart cavities.

3. Cardiac Electrophysiology

After detailing the navigation aspect, we now focus on the second crucial aspect of our simulation: the cardiac electrophysiology. The cardiac electrophysiology aims at studying the electrical activity taking place in the heart walls. This cardiac activity consists in electrical waves propagating through the myocardium. These waves correspond to local ion exchanges between cardiac cells through the cell membranes. Myocardial cells are therefore polarized, i.e. there is a potential difference between the inside and the outside of the cells. This potential difference is called transmembrane potential. Electrically isolated from the atria by a collagen layer, ventricular depolarization is induced by a specific area connecting atrial and ventricular chambers: the atrio-ventricular node. The stimulus propagates through a specific path inside the myocardium: from the bundle of His to the Purkinje fibers, through the Purkinje-myocyte junction. This whole electrophysiological cycle triggers the muscle contraction, thus allowing proper blood flow.

Several mathematical models exist to simulate the cardiac electrophysiology. They can be sorted into three different classes: (i) ionic models, which are complex models including the different ionic concentrations and channels, involving many parameters and simulating the electrophysiology at the cellular level ten Tusscher et al. (2004); (ii) phenomenological models, which are simplified models FitzHugh (1961); Aliev and Panfilov (1996); Fenton and Karma (1998); Mitchell and Schaeffer (2003) derived from the ionic models, involving less parameters and capturing the action potential shape and its propagation at the organ level; Similar to ionic models, phenomenological models require an additive diffusion term to simulate the propagation of the action potential. (iii) Eikonal models Keener (1991), which correspond to static non-linear partial differential equations of the depolarization time derived from the previous models. These models cannot accurately account for complex physiological states (such as reentries).

In the context of a training simulator, the simulation of cardiac electrophysiology must be real-time while preserving accuracy to allow user interactions. First, the electrophysiology model is briefly introduced, then all interactions allowed with this electrophysiology model are developed.

3.1. GPU Electrophysiology Model

Our work is based on the Mitchell and Schaeffer (2003) model (noted MS model) since (*i*) it has only 5 parameters, (*ii*) each parameter has a physiological meaning and (*iii*) it provides a better estimation of the action potential compared to other phenomenological models (as the Aliev and Panfilov (1996) model). Detailed in Eq. 4, the MS model is a two-variable model derived from the Fenton Karma model. Since it only captures the transmembrane potential V_m, the MS model is a "mono-domain" model. Only "bi-domain" models can simulate both intra-cellular U_i and extra-cellular potentials U_e, where $V_m = U_i - U_e$.

$$\begin{cases} \partial_t V_m = div(D\nabla V_m) + \dfrac{zV_m^2(1-V_m)}{\tau_{in}} - \dfrac{V_m}{\tau_{out}} + J_{stim} \\ \partial_t z = \begin{cases} \dfrac{(1-z)}{\tau_{open}} & \text{if} \quad V_m < V_{gate} \\ \dfrac{-z}{\tau_{close}} & \text{if} \quad V_m > V_{gate} \end{cases} \end{cases} \tag{4}$$

where V_m is the normalized transmembrane potential and z is the gating variable associated to the potassium ion influx, thus depicting the repolar-

ization phase. The diffusion term is defined by a 3x3 diffusion tensor D. τ_{open}, respectively τ_{close}, governs the gate opening, respectively gate closing, depending on the change-over voltage V_{gate}. Finally, the term $J_{stim}(t)$ is a source term. The default values of these parameters are given in Mitchell and Schaeffer (2003).

To increase computation efficiency, the electrical activity of the heart is only simulated for the ventricles. This consideration is acceptable since atria and ventricles are electrically isolated as mentioned previously. In our model, the stimulation is therefore induced by the Purkinje fibers. The implementation of Eq. 4 relies on the FEM. As explained in Subsection 2.2.1, the ventricular electrophysiology is computed on a static mesh using 30,807 linear tetrahedra. Moreover, the implementation of the weak form of reaction diffusion equations leads to zero Neumann boundary conditions, i.e. the electrical current is null in the orthogonal direction of the border. Based on our previous work Talbot et al. (2013a), the entire electrophysiology model is implemented on GPU. The simulation time step is constrained by the coarseness of the mesh. In this simulation, we use a full explicit backward differentiation (BDF) integration scheme. Due to the diffusion, the time step must remain below $dt_E \leq \frac{dx_{min}}{2\ CV_{max}} = 3 \cdot 10^{-4}$ s where dx is the smallest edge length and CV the conduction velocity inside the tetrahedron. The ionic current defines a stability limit $dt_E \leq \frac{\tau_{in}\tau_{out}}{\tau_{in}+\tau_{out}} = 2.8 \cdot 10^{-4}$ s. We use a time step $dt_E = 10^{-4}$ s compatible with both stability conditions.

We run the electrophysiology simulation alone on a NVidia GTX 580 card. Using our implementation, one cardiac cycle (0.92 s) can be computed in less than 0.788 s, i.e. 1.15 times faster than real-time.

3.2. Interactive Model

As stated in the introduction, the ablation procedure requires exploration of the geometry and the electrophysiology of the targeted heart chamber. Based on a powerful GPU implementation, we propose new interactive features reproducing these clinical gestures: extra-cellular potential measurements, reconstruction of the endocardial surface, mapping of ventricular activation times, RF ablation as well as electrical stimulation using the catheter. The interactions using the Mentice VIST device will now be detailed.

3.2.1. From Navigation to Electrophysiology Data

In order to maintain a very high flexibility, our framework handles different meshes for electrophysiology and for navigation. However, the electro-

physiology computation requires information from the catheter collision in order to allow interactions using the catheter. Measurement of the extra-cellular potential, electro-anatomical mapping, RF ablation and catheter stimulation are only possible when the catheter is in contact with the endocardium. The communication between electrophysiology and navigation is eased by the use of coherent meshes (i.e. unchanged topology), as explained in Section 2.2.1. The mapping developed between electrophysiology and navigation is now detailed.

While navigating inside the heart cavities, the collision detection returns each triangle τ_N of the navigation mesh colliding with a point of the catheter noted P. Using different meshes for navigation and electrophysiology requires finding the corresponding triangle τ_E of the electrophysiology mesh that includes the projection of P on the electrophysiology mesh. To start the search, we use a look-up table that associates the closest triangle of the electrophysiology mesh τ_E^{close} to each triangle of the navigation mesh. This look-up table is precomputed before the simulation starts. Moreover, the table remains valid during the simulation since the navigation mesh is coherent during the animation. From this initial guess τ_E^{close} given by the table, we look for τ_E regarding the barycentric coordinates of the projection of P. The desired triangle τ_E finally corresponds to the triangle having all barycentric coordinates positive. In this process, the use of the precomputed look-up table makes the catheter interaction more efficient.

3.2.2. Extra-Cellular Potential Measurement

During the procedure, cardiologists use catheters to interpret the electrical activity of the heart. These catheters can measure either unipolar or

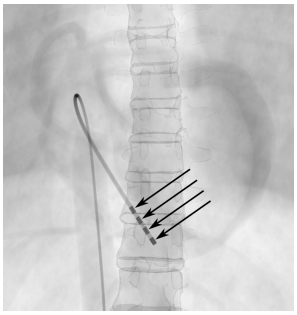

Figure 8: Fluoroscopic view of four electrodes (arrows) at the distal extremity of the catheter: each pair of electrodes measuring a bipolar extra-cellular potential

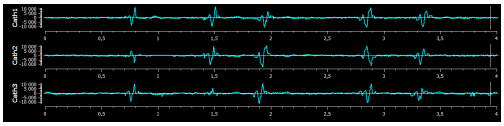

Figure 9: Three bipolar signals virtually measured by the four electrodes located along the catheter tip

bipolar potentials, respectively measuring the extra-cellular potential U_e or a difference of extra-cellular potentials ΔU_e. Bipolar potentials are often preferred as they remove the far field potentials and provide sharper depolarizations. Since the MS model is mono-domain, the four-electrode catheter (shown in Figure 8) only records transmembrane potential.

A realistic modeling of the displayed signals is key for our training simulator since cardiologists mainly rely on electrophysiological signals to understand the cardiac arrhythmia and guide the ablation procedure. The transmembrane and the extra-cellular potentials share the same timing of depolarization and repolarization events. A recorded extra-cellular measurement can therefore be mapped on the simulated transmembrane potentials based on this timing information. Real unipolar signals acquired at CHU Bordeaux are thus mapped to enable a realistic signal display.

Each consecutive pair of electrodes thus computes one bipolar signal obtained by the difference of the two unipolar signals. The resulting bipolar signals acquired *in silico* are presented in Figure 9. In the simulation, four electrodes are defined along the catheter tip and three bipolar signals ("Cath1", "Cath2" and "Cath3") can be displayed. If one of the electrodes loses contact, noisy measurements are displayed instead. If both electrodes are in contact with the endocardium, a bipolar signal is computed and drawn.

3.2.3. Electro-Anatomical Mapping

Once inside the targeted cardiac chamber, the electro-anatomical mapping starts in order to localize the arrhythmic substrate, here an ectopic focus. Using a button on the Mentice device, the user can trigger the reconstruction of the endocardial surface. As with a real mapping system, the position of the catheter is tracked and the endocardium is partially reconstructed when the catheter touches the heart wall. In other words, as soon as a collision between the catheter and the endocardium occurs, the intersected triangles of the navigation mesh are displayed. Noise is added, so that the reconstructed surface looks realistic. The surface resulting from the virtual

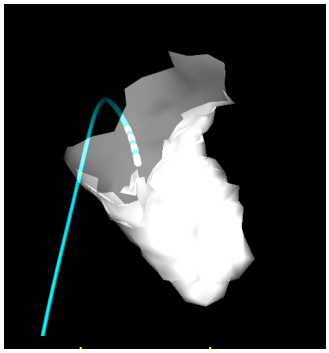

(a) Reconstruction of the 3D RV endocardium

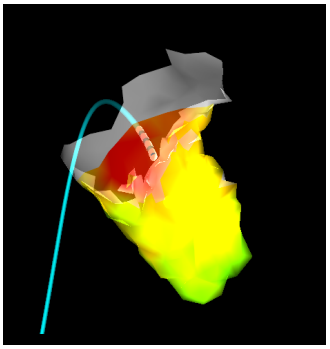

(b) Extrasystolic activation times plotted on the reconstructed surface

Figure 10: Simulated electro-anatomic mapping done in two steps: endocardial surface reconstruction, then mapping of the extrasystolic activation times (red corresponds to short activation times)

reconstruction is shown in Figure 10(a).

After reconstructing the endocardium, the simulation allows the building of a map of activation times based on the extra-cellular measurements. When an ectopic beat is detected while mapping, the activation time at the contact point with the catheter tip is saved and mapped on the endocardial surface. This activation time is based on the on-going ectopic beat and corresponds to the elapsed time between the depolarization of the ectopic focus and the depolarization of the point currently in contact with the catheter. By measuring point-by-point the extrasystolic activation times on the endocardium, the cardiology trainee can thus determine the exact location of the arrhythmia. The Figure 10(b) captures this electro-anatomical mapping simulated during our virtual procedure.

3.2.4. RF Ablation

Once a target region has been identified, the cardiologist performs the RF ablation by heating the tissue using a RF (usually from 300 to 700 kHz) alternating current. This energy is delivered through an electrode in contact with the target tissue. When the temperature exceeds 60^oC, denaturing of proteins leads to a cellular death with coagulation necrosis. To be efficient, the temperature must nevertheless not exceed 100^oC. After ablation, cardiac cells lose their electrical conductivity. As a consequence, a successful proce-

dure assumes that the regions originally responsible for the electrical disorder are well electrically isolated.

In our simulation, the ablation is modeled by a progressive decrease of conductivity in the myocardium. When the catheter tip is in contact with the heart walls, the user can trigger the RF ablation by pressing a pedal provided with the tracking device. The collision algorithm thus detects the triangle in contact with the catheter tip and its associated tetrahedron. The RF ablation is modeled by decreasing iteratively the conductivity of the associated tetrahedron. More precisely, the tetrahedron conductivity follows a decreasing function $d(t, \tau_0) = d_0 cos(\frac{\pi t}{2\tau_0})$ where d_0 is the initial conductivity and τ_0 is a time constant controlling the time required to ablate a myocardial tissue. By setting this time constant τ_0, the power of ablation can thus be adjusted to make the ablation process faster or slower. When the time of ablation reaches τ_0, the conductivity of the tetrahedron is zero corresponding to an ablated state. Then, its neighboring tetrahedra are gathered and the same decreasing function is applied to this set of tetrahedra. The electrical conductivity of the tissue is consequently updated in real-time. Moreover, the longer the ablation duration, the larger the ablation area.

3.2.5. Stimulation

In the MS equation 4, the term $J_{stim}(t)$ is a stimulation current that can be added in the equation. This nodal term is used to apply any stimulation. Since we focus on ventricular extrasystole, there are three possible current sources. All sources are independent and are not mutually exclusive, i.e. can occur simultaneously.

- First, the heart has its own natural pacemaker called the SA node. These specific cardiac cells generate a regular electrical impulse (action potential) that propagates inside the atria. Since we only consider the ventricular electrophysiology, a regular stimulus is simulated starting from the Purkinje fibers at the apex of the heart. As in Mitchell and Schaeffer (2003), we assume the stimulation current to be:

$$v_{stim} \approx \int J_{stim} dt \tag{5}$$

$$v_{stim} = 0.1 \tag{6}$$

- Second, the ectopic focus is the pathological area that causes random premature heart beats. This abnormal stimulation has also to be taken

into account using an irregular current in the ectopic region. During the calculation, a stimulus current $J_{ectopic-stim}(t)$ is irregularly applied to the nodes characterizing the ectopic focus.

- Finally, the catheter can generate electrical impulses. This stimulation can be used by the cardiologist to assess the success of the ablation procedure. When the catheter touches the heart wall, an electrical current can be delivered in the region of contact. Moreover, the current value of this catheter stimulus $J_{cath-stim}(t)$ is interactively set by the user. As for the ablation, the stimulation is triggered by the user using the second pedal of the Mentice device. If no abnormal activity is detected during the stimulation process, the arrhythmic substrate is successfully ablated.

4. Integration of Electrophysiology and Navigation Simulations

The first challenge is to run both catheter navigation and the cardiac electrophysiology together while keeping computation times close to real-time. Even if each separate simulation runs in real-time (depending on the number of contacts for the navigation), a serial execution of navigation and electrophysiology would result in low performances. Second, data have to be shared between navigation and electrophysiology to make user interactions possible. Therefore, both models have to communicate despite running at different time steps.

In this section, a powerful multithreading approach is presented that manages an asynchronous coupling while keeping good performances. Then, details are given about the graphical user interface, specifically designed to increase the sense of immersion.

4.1. Multithreading Approach

To integrate both electrophysiology and navigation simulations, we exploit the CPU parallelism and we choose a task scheduling architecture. This technique is an efficient way to scale the computation to all the CPU cores available.

The work load is broken down into tasks and a scheduler maps the tasks on each individual CPU. A task is a block of code that executes a fraction of the work independently of other tasks and can run concurrently. The scheduler creates a thread for each processor, manages the thread synchronization and

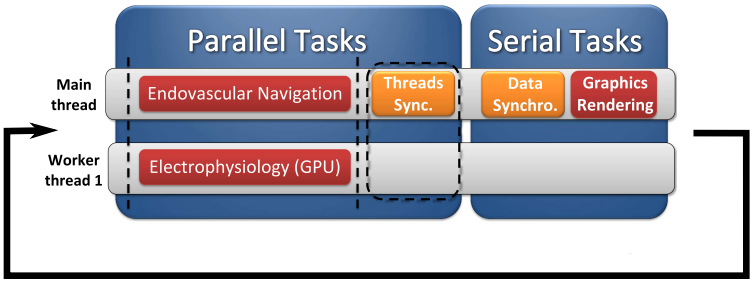

Figure 11: Multi-thread architecture: asynchronous navigation and electrophysiology threads, with a serial graphics rendering

maps the task execution into threads, finding a new task to start when one ends.

4.1.1. Main Simulation Tasks Design

We know the electrophysiology computation is carried out onto GPU and it has been noted that the graphics task is only a small fraction of the computation time. From these observations, we built our specific multithreading architecture. As detailed in Figure 11, the main loop of our multithreading architecture is split into a parallel part executing concurrently the endovascular navigation and electrophysiology simulations and a serial part executing the graphics rendering.

Electrophysiology simulation requires a very low time step $dt_E \leq 1.5 \cdot 10^{-4}$ s for stability reasons, whereas navigation simulation is running with $dt_N \leq 0.02$ s. Based on our multithreading structure, several time integration loops of the electrophysiology are computed in the electrophysiology task whereas only one step is performed for the navigation. We assessed that 175 integration steps of electrophysiology for one step of navigation with a global time step $dt_N = 0.02$ s is the best compromise, i.e. for electrophysiology $dt_E = 1.15 \cdot 10^{-4}$ s. Our framework can then be depicted as an asynchronous simulation based on multithreading.

4.1.2. Communication between Tasks

The challenge in multithread design resides in handling the data synchronization between concurrent tasks. An optimal implementation assumes to find the best trade-off between avoiding the increase of the serial execution time and avoiding the use of synchronization locks.

To avoid the use of synchronization locks, each main task has its own copy of the data. Data synchronization is performed before the graphics task, as it appears in Figure 11. The choice of running the graphics task serially prevents data synchronization between graphics and the other main tasks, thus reducing the amount of data exchange after each simulation loop.

During the step of data synchronization, few data are exchanged, as summed up in Figure 12. First, the tracking device must pass on information regarding the catheter motion to the navigation part, and update information about user interactions for the electrophysiology part. Secondly, the electrophysiology thread needs to recover all collision information, so that the user can interact with the patient electrophysiology using the catheter.

4.2. Graphical User Interface

To increase the realism of our training system, a graphical user interface (GUI) inspired by the setup inside the operating room (Figure 2(a)) is designed. Radiology interventions for RF ablation of cardiac arrhythmia are usually based on three main information sources:

- fluoroscopic images, sporadically acquired when the cardiologist needs them. These images are displayed on a dedicated screen.
- electrical signals, gathered on one unique screen. As mentioned previously, these signals are key in the procedure to detect the abnormal electrical activity of the ectopic focus.

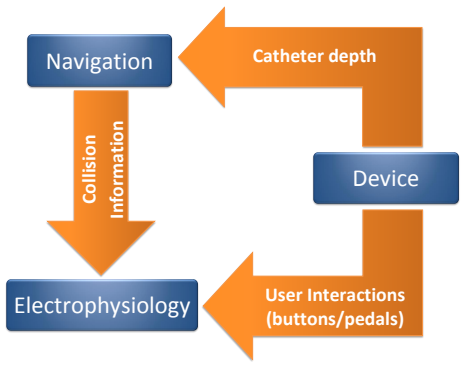

Figure 12: Exchange of data during data synchronization that is crucial for user interactions

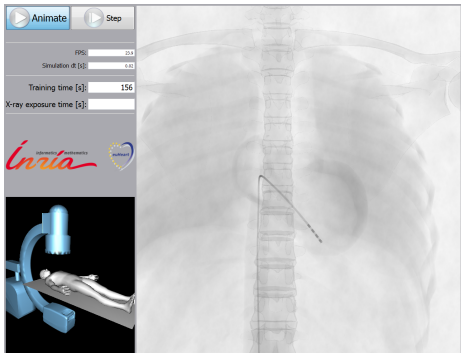

(a) Viewport n^{o}1: fluoroscopic imaging

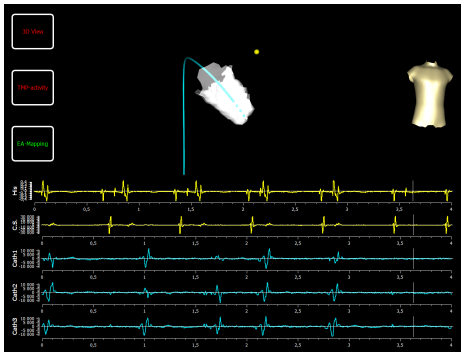

(b) Viewport n^{o}2: electro-anatomical mapping and signals

Figure 13: View of the two screens used in our training simulator

- a 3D electro-anatomical map including the moving catheter. During real intracardiac interventions, the 3D endocardial surface is reconstructed by tracking collisions between the catheter and the heart walls. The simulator described in Chiang et al. (2013) achieves a virtual reconstruction of the anatomical model of a ventricle. Our simulation reproduces not only the endocardium reconstruction but the mapping of activation times as well. From the analysis of this activation map, the ectopic focus can thus be located.

Our GUI mimics the layout of an operating room and incorporates the equivalent information available during the procedure. A global view of our GUI is shown in Figure 13.

- **Viewport n°1**: includes all the buttons controlling the simulation. This screen is also used to display the fluoroscopic images. The image orientation can be changed by moving the C-Arm, controlled by the tracking device. Joysticks of the Mentice device can be used to move the C-Arm and translate the operation table. Additional information regarding the training is displayed, such as the total duration of the training session or the ablation duration.

- **Viewport n°2**: provides a 3D view for the electro-anatomic mapping and a set of intra-operative measurements. The 3D view includes the catheter moving inside the cardiovascular system. The reconstruction

of the static endocardium and the mapping of activation times are displayed in this second viewport. Another visualization mode including the 3D dynamic cardiac electrophysiology is available (as shown in Figure 14, thus helping cardiology trainees to better understand the pathology at the organ level. With this mode, the GPU computation of the transmembrane potential (see subsection 3.1) that runs permanently becomes visible. This viewport also shows all the different recorded signals: signals at specific anatomical points (His bundle, coronary sinus) or the signals measured by the catheter.

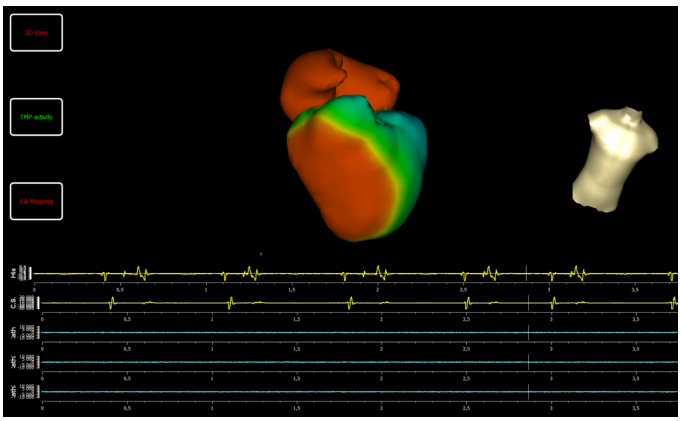

Figure 14: 3D visualization of the MS model of cardiac electrophysiology

5. Results

5.1. Simulation Scenario

The designed training involves a virtual patient suffering from a cardiac arrhythmia caused by an ectopic focus. This scenario assesses the ability of our simulator to reproduce a complete ablation procedure and to account for user interactions. As detailed previously, the ablation procedure for ectopic focus can be divided into three parts: catheter navigation, localization of the diseased region and ablation. Each step will now be presented and illustrated.

Navigation. First, the user has to navigate using the catheter from the femoral vein to the RV where the ectopic focus is located. After guiding the catheter through the vena cava (see Figure 15(a)), the catheter enters the

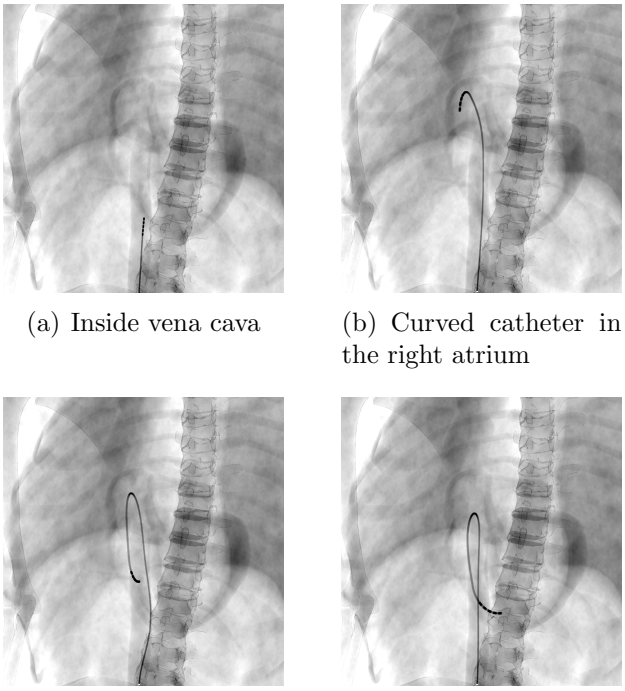

(a) Inside vena cava

(b) Curved catheter in the right atrium

(c) Inside the right ventricle

(d) Final position

Figure 15: Intra-cardiac catheterization

heart. However, the RV is not straightforward to reach from the vena cava. To manage this, cardiologists normally use a bending catheter in order to orientate its tip towards the tricuspid valve and thus enter the RV easily. During the virtual procedure, the user faces the same issue and needs to bend the catheter to face the RV (see Figure 15(b)). As in a real operation, it can be experimentally noticed that bending the catheter makes the RA-to-RV navigation easier in the simulation. Finally, the RV can be accessed by further inserting the catheter, as described in Figure 15(c) and Figure 15(d). This framework therefore includes a faithful catheter navigation step that strongly matches the ablation procedure.

Localization. Once inside the RV, the ectopic focus needs to be localized. This diseased area generates irregular extrasystolic stimuli. A capture of ectopic beats during the simulation is shown in Figure 16. In case of a ventricular extrasystole, the ectopic pattern is characterized by an early depolarization of the ventricle (visible on the catheter bipolar measurements). To start the localization, the endocardium must first be reconstructed. The user must slide the catheter against the heart wall to reconstruct a 3D surface (see Figure 10(a)). Using an electrophysiology mapping, it is possible to locate the ectopic focus by studying the activation pattern produced by an extrasystolic beat. The pathological area can be found by iteratively measuring activation times on the endocardial surface. The ectopic focus should be the region with the shortest activation time. After acquisition of extrasystolic activation times on the endocardium, Figure 10(b) reveals the ectopic focus in the red area.

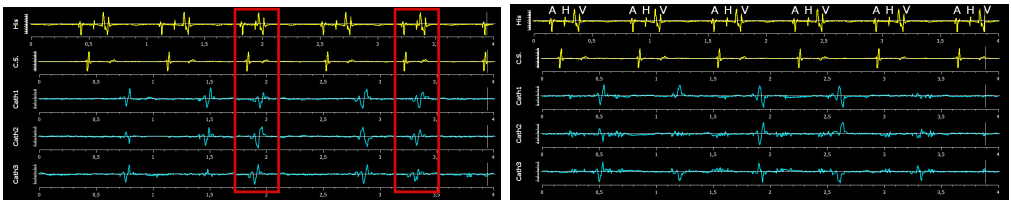

(a) Ectopic beats (red rectangles)

(b) Sinus rhythm after ablation of the ectopic focus: with regular atrial (A), His bundle (H) and ventricular (V) activations

Figure 16: Signals available in the simulation: with His bundle and coronary sinus measurements in yellow; and the three bipolar signals from the catheter

Ablation. As soon as the ectopic region is localized, the user can proceed with RF ablation. While ensuring contact between the catheter and the endocardium, the user can deliver the alternating current by pressing the left pedal. The scar resulting from the ablation is shown in Figure 17.

The success of the ablation resides in isolating the complete region responsible for the ectopic beats. Therefore, abnormality in the cardiac rhythm should not be observed anymore and a regular sinus rhythm should remain, as it appears in Figure 16(b). To assess the success of the ablation, the user can deliver electrical impulses at different frequencies using the catheter. If no ectopic activity is detected, the entire region responsible for the ectopic

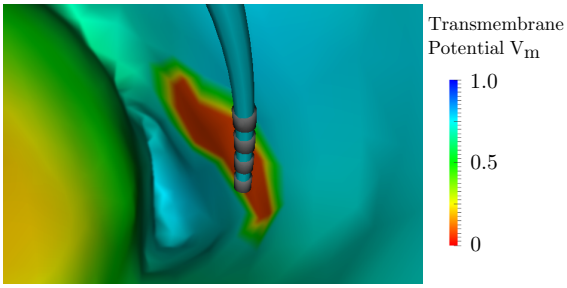

Figure 17: Internal view of the RV: colors correspond to the transmembrane potential; the red area underwent ablation

beats is ablated and the operation is a success. However, if abnormal beats appear again, the ectopic focus is only partially ablated and the procedure must be completed.

5.2. Performances

Exploiting the power of both multithreading and GPU computing, we achieve a fully interactive simulation. Our simulation runs on a computer including an Intel Core i7 CPU and an NVidia GTX 580 GPU. The performance results are given in Table 1 regarding the different steps during the procedure. In this table, real-time ratio stands for the ratio of elapsed time over computation time. When the simulation is faster than real-time (ratio $>$ 1), the computation can be slowed down to retain real-time. From Table 1, we first realize that the computational efficiency is strongly related to the number of contacts, i.e. to the navigation part. At the beginning of the procedure, only few contacts are detected whereas, once inside the heart, the catheter leans against the endocardium, thus decreasing the performance. This reveals that the navigation part tends to limit the overall performance when many contacts (over 50) are detected. 50 contacts implies 150 constraints which is substantial regarding the number of beams in our model (40 beams).

Table 1 also shows that our training system runs between 1.1 and 2.3 times slower than real-time. Our hybrid architecture proves to be efficient so that the entire simulation remains interactive. All possible interactions were introduced in Section 3.2 and illustrated in Section 5.1. Another crucial feature regarding our scope is that these interactions do not affect the performances. As a consequence, this training simulator for cardiac RF ablation

procedure already offers close to real-time performances and a high level of interactivity.

			Navigation only		Training Simulator	
Position	**Nb of contacts**		**FPS**	**Real-time ratio**	**FPS**	**Real-time ratio**
	Mean	**[min-max]**				
Start	0	[0 - 0]	70.3	1.41	44.0	0.88
Vena cava (see Figure 15(a))	2	[2 - 2]	67.3	1.35	43.8	0.87
Entrance of atrium	5	[2 - 14]	62.3	1.25	31.6	0.63
Loop (see Figure 15(b))	110	[98 - 125]	26.4	0.53	21.5	0.43
Final (see Figure 15(d))	50	[41 - 65]	45.9	0.92	23.6	0.47

Table 1: Performance results of the navigation simulation separately, and for our whole training framework (using for both a time step $dt = 0.02$ ms)

5.3. Clinical Evaluation

An evaluation of our training simulation has been performed in the cardiology department at Guy's and St Thomas' National Health Service in London. At this occasion, seven electrophysiologists with different level of experience practiced a virtual RF ablation of an ectopic focus. It included the navigation of a catheter from the femoral vein to the RV, a 3D reconstruction of the RV, a mapping of activation times and eventually the ablation itself. In the group, 4 participants presented themselves as novice (less than 3 years of learning with almost no clinical practice) and 3 were experts (more than 10 years of clinical experience). The evaluation protocol started with a presentation of the user interface and the objectives of the exercise. After their virtual experience, cardiologists evaluated the simulator by rating the different features of the simulator using specific grades (see Table 2).

The study focuses on five main items. First, the "Procedure Evaluation" assesses the ability of the user to perform different tasks of the scenario. Second, the realism of the physical modeling (behavior of the catheter, ablation

	Grade
Failed	0.0
Not satisfactory, to improve	1.0
Good	2.0
Very Good	3.0

Procedure Evaluation	**Mean Grade**	**Std. Dev.**
Able to navigate through the venous system with the catheter	2.25	0.57
Able to bend the catheter and reach the RV	1.75	0.70
Able to reconstruct the RV endocardial surface	2.67	0.53
Able to map the activation times on the surface	2.30	0.76
Pathology can be characterized based on electrical measurements	2.30	1.02
Able to locate the ectopic focus using the intra-operative electrical measurements	2.10	0.49
Ablation can be performed	2.10	0.49
Able to ablate the ectopic focus	2.10	0.49
Realism of the Simulation	**Mean Grade**	
Heart Motion	2.33	0.50
Fluoroscopic imaging	2.50	0.97
Catheter navigation	2.00	0.22
Electrophysiological signals	2.25	0.89
3D Mapping Simulation	2.50	0.67
Ablation procedure	2.33	0.63
Sensitive feedback	1.75	0.89
Interactivity of the Simulation	2.67	0.67
Immersive Experience	2.50	0.67
Global Experience	2.50	0.67

Table 2: Results of the clinical survey assessing our simulator

model), the 3D and fluoroscopic rendering and the signals are evaluated in the item "Realism of the Simulation". A third grade must be given for the level of "Interactivity of the Simulation" corresponding to the responsiveness of the simulation, which relates to the computational efficiency of the system. To quantify the feeling of treating a real patient, the user must provide a grade for the "Immersive Experience". A last grade is required to evaluate the simulator as a whole.

From this survey, it appears that the two worst features of the simulator are: (i) reaching the RV from the RA by bending the catheter and (ii) the tactile feedback. For the first issue, some clinicians experienced difficulties while looping in the RA due to the radius of curvature of the catheter tip. Following this evaluation, the shape of the steerable catheter has been adjusted by increasing the radius of curvature. Second, electrophysiologists pointed out a lack of force feedback using the catheter, especially when the catheter hits the heart walls. So far, no force feedback has been implemented in our simulation. During the evaluation process, clinicians also pointed out that displaying a surface ECG could help the interpretation of the catheter electrical signals. The implementation of both force feedback and surface ECG remains a future work.

Features obtaining the best grade are the 3D reconstruction of the endocardium and the global level of interactivity in the simulation. These positive appraisals attest the good combination of catheter navigation and collision detection once inside the ventricle. It also demonstrate the ability of our architecture to reach performances allowing the simulation to remain responsive although close to real-time. Moreover, the average grade given to this virtual experience amounts to 2.50, which is very encouraging.

Regarding the standard deviation information, the grade $2.00^{\pm 0.22}$ for the navigation simulation highlights the realistic physical behavior of the catheter. This also validates the simplification of uni-directional collision response. Electrophysiologists agreed on the good level of interactivity during the steps to locate the ectopic focus and ablate it giving a grade of $2.10^{\pm 0.49}$. Large deviations are observed for the interpretation of the electrical measurements with a grade of $2.30^{\pm 1.02}$. Half of the involved electrophysiologists asked for additional electrograms. During the procedure, clinicians are used to interpret surface ECG in addition to the His bundle, coronary sinus and catheter measurements. The fluoroscopic imaging received a grade of $2.50^{\pm 0.97}$ denoting a strong disparity among the participants in the evaluation. Two electrophysiologists expected to see the moving catheter overlying

on static fluoroscopic images when no fluoroscopic image is acquired.

5.4. Discussions

Although the simulation always remains fully interactive, the computational power dedicated to the endovascular navigation significantly increases when leaning against the atrium. To improve the performance of the collision detection, our algorithm could be implemented on GPU. Decreasing the density of beam elements of the catheter could reduce the number of contacts, but this would affect the stability of the simulation. Alternative methods for collision detection could be used, such as implicit surfaces for navigation using blubby models Yureidini et al. (2012), or distance maps. The definition of dynamic implicit surfaces corresponding to the endocardium would be extremely challenging, but dynamic distance maps (4D) would be an interesting alternative.

In the simulation of endovascular navigation, the main challenge for performance resides in the computation of the collision response. The use of a contact/friction model for the collision response is key to have realistic behavior of the catheter during the simulation, but other collision response methods are envisaged in the literature. Simplified models, such as the penalty method developed by Luboz et al. (2009), can be used but would decrease the realism of the catheter navigation. Catheter contact can also be efficiently solved using contact groups, as described by Talvas et al. (2015). Collision response can then be computed in parallel using a usual Gauss-Seidel solver.

For the electrophysiology, we present an efficient GPU version of the Mitchell Schaeffer model. However, the heart contraction is precomputed based on patient data and therefore irrespective of the electrophysiology patterns. Implementing an electro-mechanical (EM) model would increase the realism of the simulation, since any depolarization (induced by ectopic beat, or catheter stimulation) would generate a specific mechanical contraction. In a previous work Talbot et al. (2013a), an EM model is developed coupling the Mitchell Schaeffer model with a Bestel-Clément-Sorine EM model. However, EM models are computationally-demanding and integrating this new feature would prevent any interactive simulation.

As mentioned previously, the clinical evaluation highlights the absence of force feedback. During the development of the simulation, opinions of the clinical experts were diverging concerning the haptic feedback while manipulating the catheter. While some clinicians attested that an elastic haptic

feedback could be felt, others considered that surgical gloves were preventing any identifiable feedback. Furthermore, the Mentice interface technology, based on brakes, only allows the rendering of friction force and not elastic force. It leads us to ignore haptic feedback in the simulator even if we already have the software components to compute haptic rendering from simulation.

Interesting feedback were collected from our first clinical evaluation. However, a new clinical evaluation involving more scenarios must be conducted. Random cases of ectopic foci could easily be built, thus avoiding a user training twice on the same case. The type of arrhythmia simulated has to be extended. To do so, new methods, as proposed in Talbot et al. (2015), have to be developed to estimate the arrhythmia-specific model parameters. A follow-up evaluation of medical trainees could quantify the efficiency of the training simulations compared to the usual curriculum.

6. Conclusion & Perspectives

In this paper, we have presented the first training system coupling an advanced catheter navigation with a fast cardiac electrophysiology model. We believe that this fully interactive framework is an important contribution towards training in cardiology based on medical simulators. The first main contribution of this work is to propose an interactive catheter navigation inside a moving venous system and a beating heart. The virtual catheterization reproduces navigation issues that can be solved using a bending catheter. Second, we introduced a real-time GPU electrophysiology model allowing interactions during the simulation such as extra-cellular potential measurement, endocardial surface reconstruction, electrophysiology mapping, RF ablation, and electrical stimulation. Third, both navigation and electrophysiology simulations were integrated within a flexible framework. An innovative management of the computational units based on multithreading offers performances close to real-time. Even inside the contracting RV, the simulation remains only twice slower than real-time. Using a GUI that mimics the interventional environment, cardiologists could therefore train on virtual ablation scenario similar to their future operating room. Finally, the clinical study conducted at the St Thomas Hospital highlights the satisfactory aspects and the weaknesses of our simulation. This framework is therefore a first step towards realistic and efficient virtual training systems in cardiology.

As future work, the implementation on GPU of the collision detection will improve the performance of the endovascular navigation. Using the future generation of catheterization hardware rendering elastic forces would meet the requirements of clinicians regarding the force feedback. Additional patient cases will be created so that trainees can train on different types of arrhythmias. With this set of scenarios, a new clinical evaluation will be conducted to assess the effect of simulation in the medical curriculum.

Acknowledgements

Authors would like thank our clinical collaborators for their significant help in optimizing and assessing the simulator, especially Aldo Rinaldi, John Whitaker, Henry Chubb from Guy's and St. Thomas' NHS, London and Darren Hooks working in the Liryc team of Centre Hospitalier Universitaire, Bordeaux.

References

Aliev, R., Panfilov, A., 1996. A simple two-variable model of cardiac excitation. Chaos, Solitons and Fractals 7, 293–301.

Aliot, E. M., Stevenson, W. G., Almendral-Garrote, J. M., Bogun, F., Calkins, C. H., Delacretaz, E., Della Bella, P., Hindricks, G., Jaïs, P., Josephson, M. E., et al., 2009. Expert consensus on catheter ablation of ventricular arrhythmias developed in a partnership with the european heart rhythm association (ehra), a registered branch of the european society of cardiology (esc), and the heart rhythm society (hrs); in collaboration with the american college of cardiology (acc) and the american heart association (aha). Europace 11 (6), 771–817.

Bartocci, E., Cherry, E. M., Glimm, J., Grosu, R., Smolka, S. A., Fenton, F. H., 2011. Toward real-time simulation of cardiac dynamics. In: Proceedings of the 9th International Conference on CMSB. ACM, pp. 103–112.

Bertails, F., Audoly, B., Cani, M.-P., Querleux, B., Leroy, F., Lévêque, J.-L., 2006. Super-helices for predicting the dynamics of natural hair. In: ACM Transactions on Graphics. Vol. 25. pp. 1180–1187.

Chiang, P., Zheng, J., Yu, Y., Mak, K., Chui, C., Cai, Y., 2013. A vr simulator for intracardiac intervention. Computer Graphics and Applications, IEEE 33 (1), 44–57.

Corporation, S. M. S., 2013. Simantha.
URL http://www.medsimulation.com/Simantha.asp

Cosserat, E., Cosserat, F., Brocato, M., Chatzis, K., 1909. Théorie des Corps Déformables. A. Hermann Paris.

Dawson, S., Cotin, S., Meglan, D., Shaffer, D., Ferrell, M., 2000. Designing a computer-based simulator for interventional cardiology training. Catheterization and Cardiovascular Interventions 51 (4), 522–527.

Dequidt, J., Marchal, M., Duriez, C., Kerien, E., Cotin, S., 2008. Interactive simulation of embolization coils: Modeling and experimental validation. In: MICCAI 2008. Vol. 5241. Springer, pp. 695–702.

Duriez, C., Cotin, S., Lenoir, J., Neumann, P., 2006. New approaches to catheter navigation for interventional radiology simulation 1. Computer Aided Surgery 11 (6), 300–308.

Duriez, C., Dubois, F., Kheddar, A., Andriot, C., 2005. Realistic haptic rendering of interactive deformable objects in virtual environments. IEEE Transactions on Visualization and Computer Graphics 12, 36–47.

Faure, F., Duriez, C., Delingette, H., Allard, J., Gilles, B., Marchesseau, S., Talbot, H., Courtecuisse, H., Bousquet, G., Peterlik, I., Cotin, S., June 2012. SOFA: A Multi-Model Framework for Interactive Physical Simulation. Vol. 11. Springer.

Fenton, F., Karma, A., 1998. Vortex dynamics in three-dimensional continuous myocardium with fiber rotation. Chaos 8, 20–47.

FitzHugh, R., 1961. Impulses and physiological states in theoretical models of nerve membrane. Biophysical Journal 1 (6), 445–466.

HealthCare, C., 2013. Cathlabvr.
URL https://caehealthcare.com/home/eng/product_services/product_details/cathlabvr

Johnson, D., Willemsen, P., 2004. Accelerated haptic rendering of polygonal models through local descent. In: Haptic Interfaces for Virtual Environment and Teleoperator Systems, 2004. HAPTICS '04. Proceedings. 12th International Symposium on. pp. 18–23.

Keener, J., 1991. An eikonal-curvature equation for action potential propagation in myocardium. Journal of Mathematical Biology 29, 629–651.

Luboz, V., Blazewski, R., Gould, D., Bello, F., 2009. Real-time guidewire simulation in complex vascular models. The Visual Computer 25 (9), 827–834.

Mansi, T., Pennec, X., Sermesant, M., Delingette, H., Ayache, N., 2011. iLogDemons: A demons-based registration algorithm for tracking incompressible elastic biological tissues. International Journal of Computer Vision 92 (1), 92–111.

Maron, B. J., Towbin, J. A., Thiene, G., Antzelevitch, C., Corrado, D., Arnett, D., Moss, A. J., Seidman, C. E., Young, J. B., 2006. Contemporary definitions and classification of the cardiomyopathies. Circulation 113 (14), 1807–1816.

Mentice, 2012. Vist.
URL `http://www.mentice.com`

Mitchell, C., Schaeffer, D., 2003. A two-current model for the dynamics of cardiac membrane. Bulletin of Mathematical Biology 65, 767–793.

Przemieniecki, J. S., 1985. Theory of Matrix Structural Analysis. Courier Dover Publications.

Rapaka, S., Mansi, T., Georgescu, B., Pop, M., Wright, G., Kamen, A., Comaniciu, D., 2012. Lbm-ep: Lattice-boltzmann method for fast cardiac electrophysiology simulation from 3d images. In: MICCAI 2012. Vol. 7511. Springer Berlin Heidelberg, pp. 33–40.

Siemens, 2006. Cathi.
URL `http://www.siemens.com/innovation/en/publikationen/publications_pof/pof_spring_2006/simulation_articles/training.htm`

Simbionix, 2012. Angiomentor.
URL http://simbionix.com/simulators/angio-mentor

Talbot, H., Cotin, S., Razavi, R., Rinaldi, C., Delingette, H., Jun. 2015. Personalization of Cardiac Electrophysiology Model using the Unscented Kalman Filtering. In: CARS 2015. Barcelona, Spain.
URL https://hal.inria.fr/hal-01195719

Talbot, H., Marchesseau, S., Duriez, C., Sermesant, M., Cotin, S., Delingette, H., April 2013a. Towards an interactive electromechanical model of the heart. Journal of the Royal Society Interface Focus 3 (2).

Talbot, H., Spadoni, F., Sermesant, M., Ayache, N., Delingette, H., January 2013b. Deliverable D10.4.2. Rapport de recherche.
URL http://hal.inria.fr/hal-00918211

Talvas, A., Marchal, M., Duriez, C., Otaduy, M., et al., 2015. Aggregate constraints for virtual manipulation with soft fingers. Visualization and Computer Graphics, IEEE Transactions on 21 (4), 452–461.

ten Tusscher, K., Noble, D., Noble, P., Panfilov, A., April 2004. A model for human ventricular tissue. American Journal of Physiology - Heart and Circulatory Physiology 286 (4), 1573–1589.

Theetten, A., Grisoni, L., Andriot, C., Barsky, B., 2008. Geometrically exact dynamic splines. Computer-Aided Design 40 (1), 35–48.

Wang, F., Duratti, L., Samur, E., Spaelter, U., Bleuler, H., 2007. A computer-based real-time simulation of interventional radiology. In: Engineering in Medicine and Biology Society, 2007. EMBS 2007. 29th Annual International Conference of the IEEE. IEEE, pp. 1742–1745.

Yureidini, A., Kerrien, E., Dequidt, J., Duriez, C., Cotin, S., Oct. 2012. Local implicit modeling of blood vessels for interactive simulation. In: Ayache, N., Delingette, H., Golland, P., Moria, K. (Eds.), MICCAI - 15th International Conference on Medical Image Computing and Computer-Assisted Intervention. Vol. 7510. Springer, Nice, France, pp. 553–560.
URL https://hal.inria.fr/hal-00741307